scientific reports

Check for updates

OPEN

Automatic LPI radar waveform recognition of overlapping signals based on vision language model

Pengkun Yang[1,2], Guangyi Li[1,2]✉, Hui Tang[1], Yingjie Zhao[1] & Hua Yan[1]

Low probability of intercept (LPI) microwave waveforms are commonly utilized in multiple radar systems. Identifying precisely the modulation formats of LPI waveform is of importance in complex electromagnetic environment. We propose a framework for recognizing overlapping LPI radar waveforms. By utilizing two distinct encoders for text and image, the model effectively aligns radar image and context prompt embeddings into a unified feature space. This alignment enables the model to more deeply learn and capture the intrinsic characteristics of radar waveforms, enhancing its ability to discern subtle modulation features. On the premise of using only single modulation signal as training data, high-precision identification of highly overlapping waveforms at random frequency bands under different noise interference levels has been successfully achieved. Experimental results show that the proposed model not only implements zero-shot classification task, but also demonstrates robustness to the variation of signal frequency bands and environment interference via Gradient-weighted Class Activation Mapping (Grad-CAM), which is more practically meaningful.

The utilization of low probability of intercept (LPI) radar systems in electronic warfare has grown exponentially due to their remarkable capabilities. These radar systems emit LPI microwave signals with ultra-low peak power, expansive bandwidth, and impressive long-range detection capabilities. These attributes make LPI radars highly effective in scenarios where stealth and detection over large distances are paramount[1,2]. As the sophistication of electromagnetic environments evolves, the complexity of signals received from various LPI radar emitters increases. These signals can be modulated in different formats, each with unique characteristics that can make them challenging to distinguish from one another. The potential for these signals to overlap in time or frequency domains further complicates the task of automatic waveform identification.

The field of automatic microwave waveform recognition has been a focal point of extensive research for many years. Early studies have predominantly concentrated on identifying radar signals that employed a single modulation type[3–8]. In these studies, feature extraction is either manually performed by experts with specialized knowledge[3,4] or is facilitated by deep learning strategies[5–8]. The manual approach, while potentially effective, is not always feasible in real-world scenarios due to the need for highly skilled personnel. The advent of more powerful computational hardware has propelled deep learning to the forefront of feature extraction methodologies. However, the features of overlapping signals are not easily extracted through manual methods or even with models initially designed for single modulation signals. The complexity of extracting comprehensive features from overlapping LPI signals necessitates the development of more advanced algorithms and models.

As for overlapping signal recognition, blind source separation (BSS) might be efficient in some scenarios[9]. BSS method firstly decomposes an overlapping signal into its constituent waveform components, and single modulation recognition methods are utilized to implement signal classification. However, prior knowledge is needed during the process of BSS, and the number of modulation types significantly affects the recognition performance. In addition, multi-class learning (MCL)[10,11], multi-label learning (MLL)[12,13], and multi-instance learning and multi-label (MIML) learning[14–16] are also investigated to address the issue of overlapping waveform recognition. As for MCL, the similarity between multiple output classes and the required computation storage of designed model notably increase as the number of modulation types increases. Every overlapping signal is handled as one instance during the process of MLL, so semantic information of different areas in one image might be omitted. Compared to MLL, MIML learning treats an overlapping signal as one bag, and one bag simultaneously involves multiple sub-instances and diverse associated labels. Correlations and interdependencies between labels are fully harnessed. MIML is an effective tool to address the difficulty of data complexity and characterize data relationships for overlapping radar signals.

[1]China Airborne Missile Academy, Luoyang 471000, China. [2]Pengkun Yang and Guangyi Li contributed equally to this work. ✉email: ligy0612@126.com

However, it should be noted that in almost all previous related studies, the frequency bands for a specific waveform are identical in both the training and test datasets. For example, in[6], the center frequency of linear frequency modulation (LFM) signals in training and test datasets both range from $2f_s/16$ to $3f_s/16$ (f_s denotes the sampling rate). Nevertheless, in realistic situation, the frequency bands of intercepted microwave signals are unknown, and the position characteristic in time-frequency distribution image might affect the automatic recognition of microwave waveforms. To further adapt to real-world scenarios, the designed model should be capable of recognizing overlapping waveforms that it has not encountered before, and in the test dataset, the center frequencies of single modulation signals within the overlapping waveforms should not be fixed.

Training a model only using single modulation signals to recognize radar overlapping signals with various modulation formats is a task that pertains to the domain of zero-shot learning. In this situation, the model is required to identify previously unseen overlapping signals. Effective solutions for zero-shot learning tasks often involve visual language models (VlMs) , such as CLIP[17]. Furthermore, in this letter, the center frequencies of the training dataset and test dataset vary randomly across multiple frequency bands. Meanwhile, signals under various signal-noise ratio (SNR) levels in test dataset not only overlap in the time domain but also highly overlap in the frequency domain. These requirement significantly escalates the complexity of automatic radar waveform identification.

To address the aforementioned issue, in this letter, we propose a framework of overlapping waveform automatic recognition. The framework effectively learns the characteristics of the waveform and improves recognition accuracy by aligning radar time-frequency distribution images and context prompt embeddings in a shared feature space. The primary objective of our proposed method is to accurately classify the modulation types of overlapping LPI radar waveforms. Specifically, we aim to identify which modulation types (LFM, Barker, Frank, Costas) are present in a given radar waveform image. The evaluation criteria are based on classification accuracy, which measures the proportion of correctly identified modulation types out of all test samples. The experimental results demonstrate that only using waveform images with single modulation format can achieve high-precision overlapping signals recognition. It should be noted that the center frequencies of single modulation signals and overlapping signals under different environment interference randomly span several bands, which manifestly improves the feasibility of the proposed model in electromagnetic interference environments.

Signal model and processing

radar overlapping signals

Provided that M independent radar transmitters which emit different waveform radar signals at the same time in the electromagnetic space. These radar signals might possess various modulation types and center frequencies. All transmitted signals in the electromagnetic space are captured by one signal radar receiver, thus the intercepted signals might overlap with each other both in time and frequency domains. The overlapping signal can be mathematically expressed as

$$S = \sum_{i=1}^{M} y_i(nT) = \sum_{i=1}^{M} a_i(nT) \exp\left(j2\pi f_i(nt) + j\varphi_i\right) \tag{1}$$

where $y_i(nT)$ denotes discrete sampled LPI signals with a possible modulation type, a_i, f_i and φ_i are amplitude, carrier frequency and initial phase, respectively. The initial phase is fixed as 0 during simulation experiment for the sake of simplicity.

If the intercepted radar signals can be composed of any modulation type, then the number of total signals can be given by

$$T = \sum_{i=1}^{M} C_M^i = 2^M - 1 \tag{2}$$

Time-frequency distribution via smooth pseudo-WVD

The original temporal signals can be transformed into two-dimensional graphical representations through time-frequency transform techniques, such as short time Fourier transform, Wigner-Ville distribution, and Choi-William distribution. These transforms provide a more nuanced view of characteristics over time and frequency, facilitating a deeper analysis.

In the letter, the time-frequency distribution images of overlapping signals are obtained via smoothed pseudo-Wigner-Ville distribution (WVD) which is formulated as

$$\mathrm{WVD}(t,f) = \int_{-\infty}^{\infty} h(\tau) \int_{-\infty}^{\infty} g(t-s) \cdot x\left(t+\frac{\tau}{2}\right) x^*\left(t-\frac{\tau}{2}\right) \exp(2j\pi f\tau) d\tau \tag{3}$$

where $h(\tau)$ and $g(t-s)$ are the frequency domain and time domain windows, respectively.

Methodology

Our proposed method for recognizing overlapping LPI radar waveforms is inspired by the essence of VLM model (VLM-LPI model). The chosen modulations of LPI radar signals are LFM, Barker codes, Frank codes and Costas codes. 4 types of single modulation signal and 11 types of overlapping signals are firstly converted into time-frequency distribution images via pseudo-WVD. When presented with a new image, the image encoder of

our model extracts feature vectors from the image, which are then compared for similarity to the feature vectors of context prompt encoded by the text encoder. The category with the highest similarity score is identified as the image classification result.

VLM-LPI model

The proposed VLM-LPI model includes a text encoder and an image encoder, as shown in Fig. 1a. During the training process, single modulation images and context prompts are respectively converted into image and text embedding vectors. Image embedding and text embedding are aligned into one shared space via contrastive learning optimization. In particular, given a batch comprising N pairs of radar waveform images and corresponding texts, the VLM-LPI model is trained to estimate the matching probabilities for all possible combinations within these $N \times N$ image-text pairs. During training, the model focuses on maximizing the cosine similarity for N true image-text pairs and minimizing the cosine similarity for the $N \times N - N$ incorrect pairs. The loss function during the training phase can be given by

$$L = -\frac{1}{2}\sum_{i=1}^{N}\log\frac{\exp\left(\cos\left(I_i, T_i\right)/\beta\right)}{\sum_{j=1}^{N}\exp\left(\cos\left(I_i, T_j\right)/\beta\right)} - \frac{1}{2}\sum_{i=1}^{N}\log\frac{\exp\left(\cos\left(I_i, T_i\right)/\beta\right)}{\sum_{j=1}^{N}\exp\left(\cos\left(I_j, T_i\right)/\beta\right)} \tag{4}$$

where I_i, T_i are the i-th of image embedding vector and text embedding, respectively; cos( ) represents the cosine similarity; β is a learnable temperature initialized at 0.5.

The test phase is shown in Fig. 1b, where the overlapping radar waveform images are transformed into the image embedding vector through the image encoder, and all possible text embeddings are obtained through the text encoder. By calculating the cosine similarity between the image embedding (I_m) and all the text embeddings (T_1, ..., T_1), the label corresponding to the maximum value is the predicted label. The process of getting the predicted label can be expressed as

$$label = \arg\max_{i}\cos\left(I_m, T_i\right) \tag{5}$$

Context prompts design

In order to adapt multi-labels classification task, the context prompts are designed to indicate what type of radar signals exist in the image.

The most commonly used prompt template is "a photo of ...". However, different context prompts might cause high embedding similarities for one overlapping waveform image which contains multiple types of radar signals if the prompt template " a photo of ..." is used . For example, the context prompts, "a photo of Barker and Costas", "a photo of LFM, Barker and Costas", and "a photo of LFM, Barker, Frank, and Costas", all have a high embedding

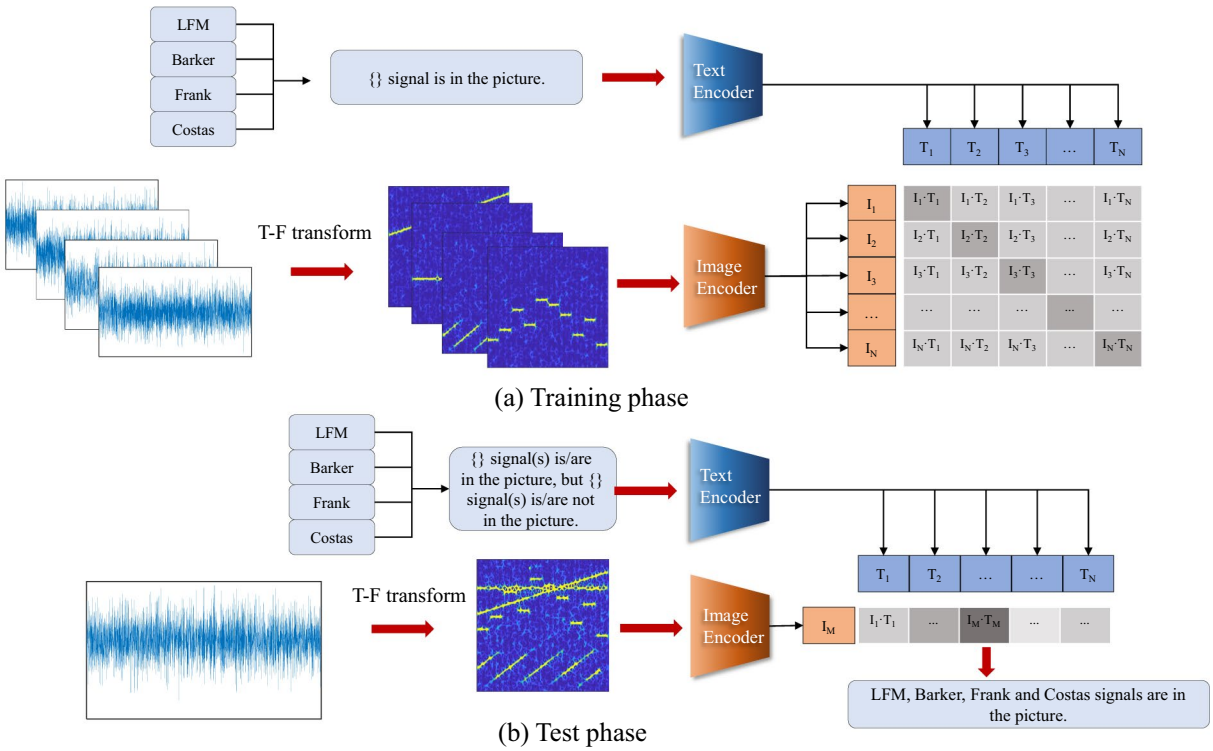


Fig. 1. The framework of the proposed framework. (**a**) Training phase; (**b**) test phase. T–F transform means time-frequency transform.

similarity for an image which only contains Barker codes and Costas codes. To address this issue and better learn the features of radar waveforms, we have designed a prompt template: "XXX signal(s) is/are in the picture, but XXX signal(s) is/are not in the picture". Under this circumstance, for an image containing LFM, Barker Codes and Costas codes, the corresponding context prompt is "LFM, Barker and Costas signals are in the picture, but Frank signal is not in the picture". In addition, it should be clarified that if all four kinds of modulation formats are in one image as shown in Fig. 1b, the context prompt is "LFM, Barker, Frank and Costas signals are in the picture."

Experiment

Experimental performance

The experimental dataset consists of four types of single modulation signal. According to Eq. (2), the total number of signal types is 15, and each combination is composed of 1000 images in our dataset. There are 4000 radar waveform images which only contains single modulation format, and the remaining images are overlapping radar waveform images which contains multiple modulation formats. 4000 single modulation signal images, and 11,000 overlapping signals are utilized as training and test dataset, respectively. It should be noted that the overlapping radar waveform data in the test dataset is regenerated, not combined from the training dataset.

In addition to simulate interference environment, the various SNR levels ranging from -10 dB to 10 dB with a step of 4 dB are added to the training and test datasets. Regarding noise power control, the SNR is defined as the ratio of the total power of the overlapping signals to the noise power, as shown in Eq. (6).

$$\mathrm{SNR[dB]} = 10\log_{10}\frac{\sum_{i=1}^{K} P_i}{P_{\mathrm{noise}}} \tag{6}$$

where P_i is the ith component signal power and P_{noise} is the noise power.

Apart from introducing noise interference into experiment, the parameters of different modulation types are adjusted. Unlike in previously related studies where the frequency band of a specific waveform is the same in both the training and testing datasets, the center frequencies of single modulation signals in the training dataset and overlapping signals in the test dataset are both randomly distributed across multiple frequency bands.

Furthermore, in the test dataset, signals not only overlap in the time domain, but also highly overlap in the frequency domain. This design not only increases the complexity of the test dataset but also evaluates the ability to recognize signals with unknown frequency characteristics. Table 1 shows the parameter used to generate the signals.

Figure 2 presents the classification accuracy for each single modulation type across different SNR levels. The results demonstrate that the proposed model maintains high accuracy even under varying SNR conditions. The accuracy for LFM, Barker, Frank, and Costas codes remain close to 100% when SNR is better than -2 dB, showcasing the robustness of the model in identifying individual modulation formats despite noise interference. This indicates that the model has effectively learned the intrinsic characteristics of each modulation type, enabling accurate recognition in diverse interference environments.

Figure 3 illustrates the classification performance of overlapping radar waveforms with multiple modulation formats across different SNR levels. The results show that the proposed model achieves high classification accuracy for various overlapping signal combinations, even under challenging conditions such as high frequency overlapping and varying SNR levels. The classification accuracy improves as the SNR increases, highlighting the model's ability to effectively distinguish between complex signal types in both low and high SNR environments. This performance underscores the effectiveness of the proposed vision-language contrastive learning approach in capturing the nuanced features of overlapping radar waveforms and demonstrates its robustness in real-world applications.

Figure 4 presents an illustrative visualization of the high-dimensional feature space via t-distributed stochastic neighbor embedding (t-SNE) when the SNR is -2 dB, showcasing the 2-D embeddings derived from our comprehensive test dataset. This dataset encompasses 11 distinct classes of overlapping radar waveforms. The features depicted in Fig. 4 are meticulously extracted from the final layer of the image encoder in our proposed model. It is observable that the disparate classes are effectively differentiated, each converging into well-defined clusters with remarkable precision. The incidence of samples mingling with clusters which do not correspond to their inherent class is rare. This visual testament highlights the profound capability of our model

Modulation type	Parameter	Range
LFM	Bandwidth	[3/20,1/5] f_s
Barker	Code length	{7,11,13}
	Number of signal periods within fixed sampling time	{1:5}
Frank	Code length	{5:8}
	Number of signal periods within fixed sampling time	{3:5}
Costas	Frequency hopping sequence length	{4,5,6,10}
	Fundamental frequency of the Costas code	[1/50,1/40] f_s

Table 1. The parameters of different modulation types. f_s: sampling frequency.

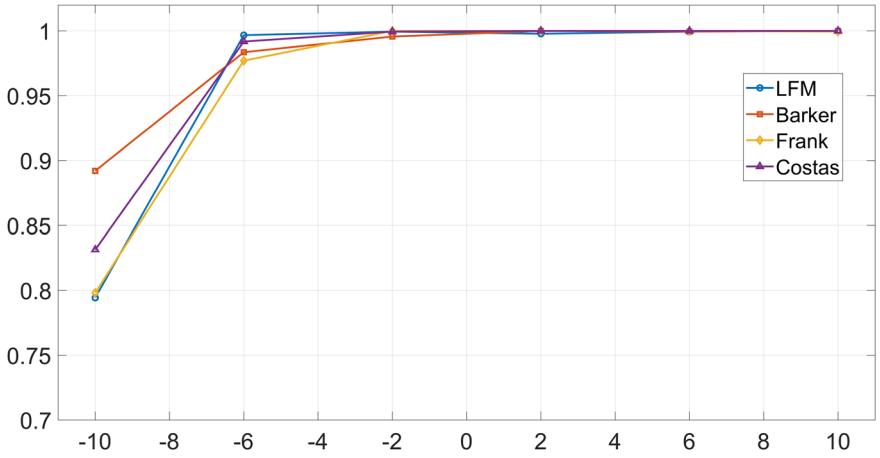


Fig. 2. Classification accuracy for single modulation signals.

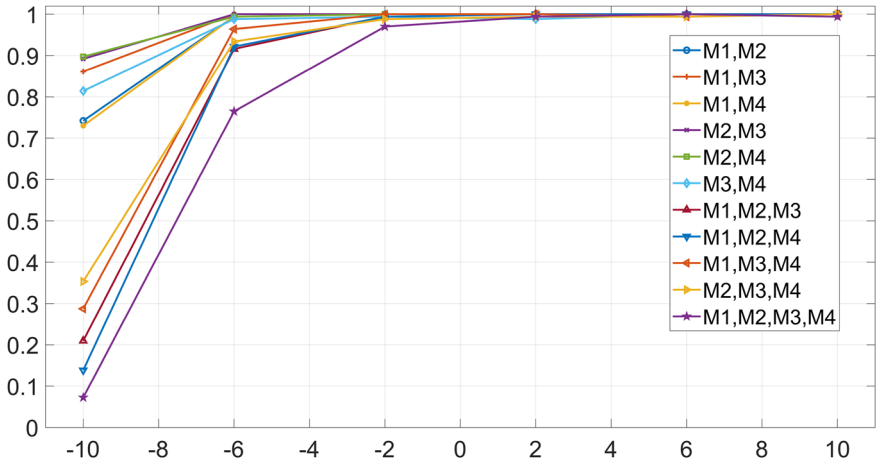


Fig. 3. Classification performance of overlapping signals with varying SNR. M1, M2, M3 and M4 denote LFM, Barker codes, Frank codes and Costas codes, respectively.

to capture and represent the nuanced distinctions between diverse signal types. The clarity of separation in the t-SNE plot validates the superior feature representation of our model.

In order to demonstrate the superior recognition capabilities of our model, Grad-CAM[18] is utilized. Grad-CAM, as an advanced visualization tool, leverages the gradient information of the model to generate Class Activation Maps (CAMs), revealing the regions of interest that the model focuses on during the decision-making process. Specifically, Grad-CAM generates a heatmap by calculating the weighted sum of the gradients of the target convolutional layer and the class activation map, which intuitively maps the areas of focus when the model processes specific inputs.

In our experiments, time-frequency diagrams for signals of different modulation types (including LFM, Barker, Frank, and Costas) are generated and Grad-CAM is used to calculate the regions of interest for the model. Figure 5 shows the original time-frequency diagrams and their corresponding Grad-CAM heatmaps. Specifically, the Raw Image in Figures 5(A)-(1)–(D)-(1) displays the original time-frequency feature diagrams containing four different waveform types. Each time-frequency diagram includes four waveforms, with their center frequencies exhibiting varying degrees of overlap.

By applying Grad-CAM technology, class activation heatmaps are successfully generated, which intuitively reveal the regions the model focuses on during classification decisions. Columns (2), (3), (4), and (5) in Fig. 5 show the heatmaps generated by the model when prompted with "LFM," "Barker," "Frank," and "Costas," respectively. The heatmaps clearly indicate that the attention of our model is concentrated on the frequency variation regions of the signals, demonstrating that our model effectively learns the key features of each waveform.

In complex environments, signals often interfere with each other, increasing the difficulty of feature extraction. Through the heatmaps generated by Grad-CAM, we can clearly observe how the model distinguishes key features of different modulation types in overlapping signals. For example, in Fig. 5(A)-(2), the LFM signal partially overlaps with the Barker signal in the time-frequency domain. However, when prompted with "LFM,"

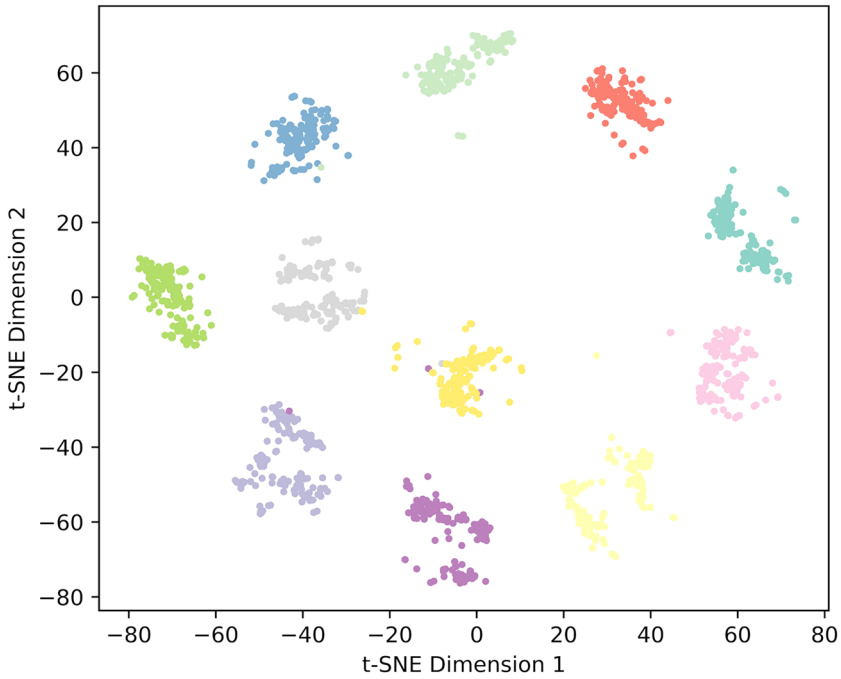


Fig. 4. Feature representation performance with t-SNE (SNR = −2 dB), each color represents one class.

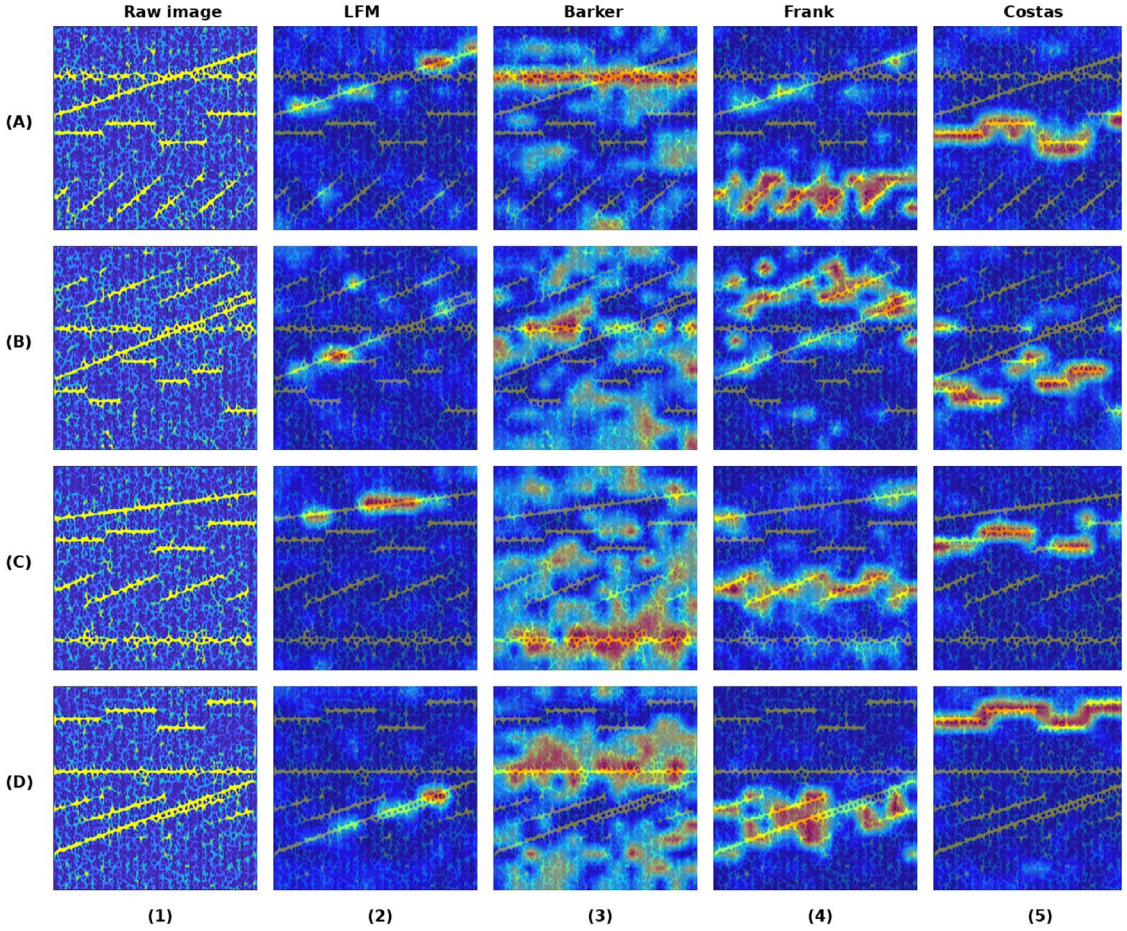


Fig. 5. Grad-CAM visualization of the attention distribution of the proposed model in identifying different overlapping radar waveforms.

Average	Vit-B/32	Vit-B/16	Resnet101
Test samples (SNR = −10)	0.3672	0.358	0.5454
Test samples (SNR = −6)	0.8901	0.9197	0.9519
Test samples (SNR = −2)	0.9842	0.9951	0.9945
Test samples (SNR = 2)	0.9929	0.9978	0.9978
Test samples (SNR = 6)	0.9902	0.9967	0.9989
Test samples (SNR = 10)	0.9918	1	0.9995
Total test samples	0.8694	0.8779	0.9147

Table 2. Performance metrics of different backbones under various SNR conditions.

the model still focuses its attention on the key regions of the LFM signal. This result indicates that our model exhibits strong robustness and feature discrimination capabilities in complex scenarios.

Ablation experiment

In our study, the performance of different convolutional neural network backbones, specifically the ResNet[19] and Vision Transformer (ViT)[20] architectures are explored. The backbones are chosen based on their covariance properties, which are pivotal for feature extraction in image-based tasks.

The results of our comparative analysis are presented in the Table 2, which illustrates the performance metrics for each backbone. The analysis of the performance data presented in Table 2 reveals that ResNet101 demonstrates a commendable performance across various SNR conditions when compared to the Vit architectures, Vit-B/32 and Vit-B/16. Despite the Vision Transformers showing high accuracy in certain SNR ranges, ResNet101 emerges as a strong contender, particularly when considering its overall average performance and its robustness in low SNR scenarios. In addition, based on the consistent high accuracy across various backbones, it can be concluded that the recognition performance of our model is robust and effective.

During training, our VLM model with ResNet-101 has around 500 million parameters, requiring substantial computational resources for contrastive learning to align image and text embeddings. However, inference time is significantly shorter, as text embeddings are fixed after training and only the visual encoder processes input images. Specifically, our framework achieves an inference time of approximately 1 millisecond per image on an NVIDIA RTX 4090 GPU, making it viable for real-time applications.

Conclusion

In conclusion, we present an innovative approach to the recognition of overlapping LPI radar waveforms by aligning the image and text embedding vectors. The proposed VLM-LPI model effectively addresses the challenges posed by the complexity of signals which are overlapped in time and frequency domains and interfered by environment noise. In our experiment, the test dataset is independently generated with distinct parameters and not a mere combination of the training dataset. Specifically, the center frequencies of single modulation signals in the training dataset and overlapping signals in the test dataset are both randomly distributed across multiple frequency bands. Moreover, the test dataset includes signals under various SNR levels. The experiment performance demonstrates enhanced robustness and adaptability in identifying LPI waveforms under the condition of zero-shot task. The VLM-LPI model offers a reliable and adaptable solution for the automatic identification and classification of complex overlapping signals in electronic warfare.

Data availability

The data that support the findings of this study are available upon reasonable request from the authors, which Guangyi Li author should be contacted if someone wants to request the data from this study.

Received: 22 December 2024; Accepted: 7 August 2025
Published online: 13 August 2025

References

1. N. Levanon, E. M. *Radar Signals* (Wiley, 2004).
2. Richards, M. A. *Fundamentals of Radar Signal Processing* 2nd edn. (McGraw-Hill, 2014).
3. Xu, C., Zhang, J., Zhou, Q. & Chen, S. Modulation classification for radar pulses in low snr levels with graph features of ambiguity function. In *2017 IEEE 9th International Conference on Communication Software and Networks (ICCSN)*. 779–783. https://doi.org/10.1109/ICCSN.2017.8230218 (2017).
4. Konopko, K., Grishin, Y. P. & Jańczak, D. Radar signal recognition based on time-frequency representations and multidimensional probability density function estimator. In *2015 Signal Processing Symposium (SPSympo)*. 1–6. https://doi.org/10.1109/SPS.2015.7168292 (2015).
5. Huynh-The, T., Hua, C.-H., Doan, V.-S., Pham, Q.-V. & Kim, D.-S. Accurate deep cnn-based waveform recognition for intelligent radar systems. *IEEE Commun. Lett.* **25**, 2938–2942. https://doi.org/10.1109/LCOMM.2021.3095278 (2021).
6. Hoang, L. M., Kim, M. & Kong, S.-H. Automatic recognition of general LPI radar waveform using SSD and supplementary classifier. *IEEE Trans. Signal Process.* **67**, 3516–3530. https://doi.org/10.1109/TSP.2019.2918983 (2019).
7. Jiang, W., Li, Y., Liao, M. & Wang, S. An improved LPI radar waveform recognition framework with LDC-UNET and SSR-loss. *IEEE Signal Process. Lett.* **29**, 149–153. https://doi.org/10.1109/LSP.2021.3130797 (2022).

8. Li, X. & Cai, Z. Deep learning and time-frequency analysis based automatic low probability of intercept radar waveform recognition method. In *2023 IEEE 23rd International Conference on Communication Technology (ICCT)*. 291–296. https://doi.org/10.1109/ICCT59356.2023.10419738 (2023).
9. Gouldieff, V., Palicot, J. & Daumont, S. Blind modulation classification for cognitive satellite in the spectral coexistence context. *IEEE Trans. Signal Process.* **65**, 3204–3217. https://doi.org/10.1109/TSP.2017.2688976 (2017).
10. Sahare, M. & Gupta, H. A Review of Multi-Class Classification for Imbalanced Data (2012).
11. Jain, P. & Kapoor, A. Active learning for large multi-class problems. In *2009 IEEE Conference on Computer Vision and Pattern Recognition*. 762–769 (2009).
12. Zhu, M., Li, Y., Pan, Z. & Yang, J. Automatic modulation recognition of compound signals using a deep multi-label classifier: A case study with radar jamming signals. *Signal Process.* **169**, 107393 (2020).
13. Zhang, M.-L. & Zhou, Z.-H. A review on multi-label learning algorithms. *IEEE Trans. Knowl. Data Eng.* **26**, 1819–1837. https://doi.org/10.1109/TKDE.2013.39 (2014).
14. Feng, J. & Zhou, Z.-H. Deep MIML network. In *AAAI Conference on Artificial Intelligence* (2017).
15. Song, L. et al. A deep multi-modal cnn for multi-instance multi-label image classification. *IEEE Trans. Image Process.* **27**, 6025–6038. https://doi.org/10.1109/TIP.2018.2864920 (2018).
16. Pan, Z., Wang, S., Zhu, M. & Li, Y. Automatic waveform recognition of overlapping LPI radar signals based on multi-instance multi-label learning. *IEEE Signal Proces. Lett.* **27**, 1275–1279. https://doi.org/10.1109/LSP.2020.3009195 (2020).
17. Radford, A. et al. Learning transferable visual models from natural language supervision. *CoRR* arXiv:2103.00020 (2021).
18. Selvaraju, R. R. et al. Grad-cam: Visual explanations from deep networks via gradient-based localization. In *IEEE International Conference on Computer Vision* (2017).
19. He, K., Zhang, X., Ren, S. & Sun, J. Deep residual learning for image recognition. In *2016 IEEE Conference on Computer Vision and Pattern Recognition (CVPR)*. 770–778. https://doi.org/10.1109/CVPR.2016.90 (2016).
20. Dosovitskiy, A. et al. An image is worth 16x16 words: Transformers for image recognition at scale. arXiv:2010.11929 (2020).

Author contributions

All authors contributed extensively to this work. P. Yang and G. Li conceived the basic idea. H. Tang, Y. Zhao, and H. Yan conducted the experiment and theoretical analysis. P. Yang and G. Li contributed to the writing of the manuscript.

Declarations

Competing interests

The authors declare no competing interests.

Additional information

Correspondence and requests for materials should be addressed to G.L.

Reprints and permissions information is available at www.nature.com/reprints.

Publisher's note Springer Nature remains neutral with regard to jurisdictional claims in published maps and institutional affiliations.

Open Access This article is licensed under a Creative Commons Attribution-NonCommercial-NoDerivatives 4.0 International License, which permits any non-commercial use, sharing, distribution and reproduction in any medium or format, as long as you give appropriate credit to the original author(s) and the source, provide a link to the Creative Commons licence, and indicate if you modified the licensed material. You do not have permission under this licence to share adapted material derived from this article or parts of it. The images or other third party material in this article are included in the article's Creative Commons licence, unless indicated otherwise in a credit line to the material. If material is not included in the article's Creative Commons licence and your intended use is not permitted by statutory regulation or exceeds the permitted use, you will need to obtain permission directly from the copyright holder. To view a copy of this licence, visit http://creativecommons.org/licenses/by-nc-nd/4.0/.

© The Author(s) 2025